

Residual correlations in liquid drop mass calculations

Jorge G. Hirsch, Alejandro Frank, and Víctor Velázquez

Instituto de Ciencias Nucleares, Universidad Nacional Autónoma de México,

Apartado Postal 70-543, 04510 México, D.F., México

E-mail: hirsch@nuclecu.unam.mx, frank@nuclecu.unam.mx, vic@nuclecu.unam.mx

Abstract

A systematic study of correlations in the chart of calculated masses of Möller and Nix is presented. It is shown that the differences between the masses calculated by Möller et al and the measured ones have a well defined oscillatory component as function of N and Z , which can be removed with an appropriate fit, reducing significantly the error width, and concentrating the error distribution on a single peak around zero. The residual correlations can have important consequences in the errors as signaling the presence of chaos, as was recently proposed.

PACS numbers: 21.10.Dr, 24.60.Lz

I. INTRODUCTION

The prediction of nuclear masses is of fundamental importance for a complete understanding of the nuclear processes that power the Sun, and the synthesis and relative abundances of the elements [1]. Möller and Nix [2], Dufflo and Zuker [3], Goriely et al [4], among many others, have developed mass formulae that calculate and predict the masses (and often other properties) of as many as 8979 nucleotides. There is a permanent search for a better parameterizations that decreases the difference with the experimental masses and produces reliable predictions for unstable nuclei.

The atomic mass excesses have been tabulated for 8979 nuclei ranging from ^{16}O to $A=339$ in [2], calculated with a finite-range droplet macroscopic model and a folded-Yukawa single-particle microscopic model. The microscopic sector includes a Lipkin-Nogami calculation of pairing gaps besides Strutinsky shell-corrections. Ground-state energies are minimized with respect to shape degrees of freedom. Only 9 constants are adjusted to the ground-state masses of 1654 nuclei, with a mass model error of 0.669 MeV in the entire region of nuclei ranging from ^{16}O to $^{263}106$.

The average mass error is found to gradually increase in a systematic way as the lighter region is approached. This behavior was related in [2] with the reliability of the Strutinsky method for the folded-Yukawa single-particle method, which is expected to be less accurate for light nuclei because the smooth, average quantities are less accurately determined from the relatively few levels occurring in light nuclei.

The significance of the difference between the measured and computed masses was interpreted from a novel perspective in [5]. A natural explanation was to propose that it originates from many-body effects not included in the mean-field scheme. The microscopic (shell-plus-pairing) corrections are split into two parts, regular and chaotic. From a semiclassical point of view, shell-effects are interpreted as modulations in the single-particle spectrum produced by the periodic orbits of the corresponding classical dynamics. The regular part was found to have fluctuations of about 3 MeV, with no mass dependence, while the fluctuations of the chaotic part are of the order of 0.5 MeV, and behave like $A^{-1/3}$. This was interpreted as an estimate of the mass fluctuations arising from neglected many-body effects. The relevance of this analysis was underlined in [1], where it was pointed out that even in the best theoretical models, it is very difficult to keep the model uncertainties lower than about 0.7 MeV, which

coincides with the order of magnitude of the expected shell energy contribution from chaotic motion.

A possible interpretation of these results is that even at ground-state level, a measurable contribution to the energy can only be calculated in a statistical sense, in the fashion of random matrix theories [1, 6]. A second component of the error would be associated with the impossibility of obtaining an arbitrary precision in the calculation of the masses, independently of the model, setting up limits which cannot be improved upon. In [7] a systematic study of masses was carried out using the shell model, in an attempt to clarify the nature of the errors. This was achieved by employing realistic Hamiltonians with a small random component.

The main motivation for the present work arose from Fig. 1, which displays the error in the 1654 isotopes of [2] and the unexpected symmetrical distribution with two peaks around the origin. This distribution was first suspected to imply a coexistence of regular and chaotic behavior, since it is possible to adjust its absolute value by means of a Brody distribution [8] with parameter $\omega = 0.4$. In this article we study the regularities in the differences between measured and calculated masses, showing that they are closely related to the presence of the double peak. Fig. 1 shows the distribution of errors obtained by Möller and Nix [2] for different distribution intervals. The intermediate figure (lines and triangles) corresponds to a distribution of 0.1 MeV where the double peak is quite evident. Enlarging the distribution

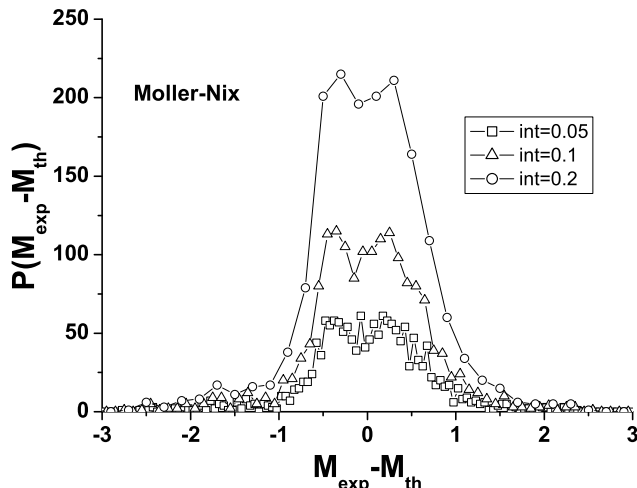


FIG. 1: Distribution of $M_{th} - M_{exp}$ Möller errors for three intervals.

interval to 0.2 MeV softens the curvature but the presence of the double peak is still very

clear. In the opposite direction, an interval of 0.05 MeV produces larger fluctuations and some apparent interference, but it is evident that the distribution still displays the peaks. We can thus conclude that the effect is real and not an artifact of a particular distribution interval.

We carried out additional tests to check the persistence of the double peak, including only nuclei with $A > 40$ and $A > 60$, normalizing the distribution according to the rule $A^{-1/3}$, and including the experimental errors. In all circumstances the double peak remained there [9].

When studying the distribution in the errors from the chart of Duflo and Zuker (DZ)[3], we do not find a double peak [9]. In the case of MN the r.m.s. error is of the order of 0.669 MeV, while for DZ the corresponding error is of 0.375 MeV. The clear difference between these two distributions, MN and DZ, begs for a more detailed analysis.

Figure 2 contains the distribution of mass differences $\Delta M(N, Z) \equiv M_{exp}(N, Z) - M_{th}(N, Z)$, (see gray code in the insert) in the $N - Z$ space, for the Möller et al. mass formula, taken from P. Möller et al.[2]. We can see large domains with a similar error (each tone is associated to the magnitude of the error). It is remarkable that very defined correlated areas of the same gray tone exist, which is a clear indication of remaining systematics and correlation.

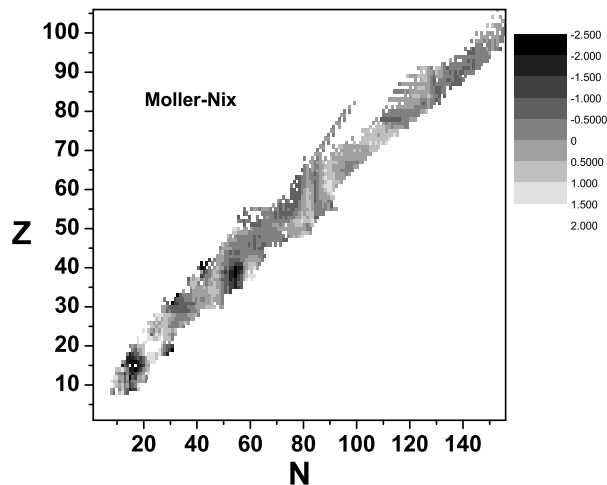


FIG. 2: Distribution of MN $M_{th} - M_{exp}$ in the $N - Z$ plane.

Both the distribution of mass errors in the N-Z plane and the presence of the double peak in the error distribution point out to the presence of important correlations which are not

taken into account in the Möller et al. mass formula. In the next sections these correlations are quantified and parametrized.

II. REGULARITIES IN THE MASS ERRORS

In order to visualize the oscillatory patterns suggested in Fig. 2, different cuts were performed along selected directions on the N-Z plane. Given the large number of chains which can be studied, we have selected those with the largest number of nuclei with measured mass. For each cut a Fourier analysis was performed, and the squared amplitudes are plotted as a function of the frequencies on the right hand side of each figure. The presence of a few frequencies with notorious large components underlines the existence of an oscillatory behavior of the mass errors.

A. Fixed N and Z

We start our analysis for fixed N or Z, i.e. we selected different chains of isotopes and isotones. Those isotopic chains with 20 or more nuclei with measured masses are presented in Fig. 3 and 4. Until 1995, the element which had most isotopes with measured masses was Cs ($Z=55$) with 34.

Fig. 3 displays the mass errors for the isotope chains $Z = 46$ to 56 , and their Fourier analysis, all exhibiting a clear peak for the low frequency $f \approx 1/20 = 0.05$.

Fig. 4 displays the mass errors for the isotope chains $Z = 30, 36, 37, 38, 40, 87, 89, 91$, and their Fourier analysis.

A similar analysis was performed for fixed N, i.e. isotonic chains, which have up to 30 nuclei with measured masses. Fig. 5 displays the mass errors for the isotone chains $N=50$ to 61 , and their Fourier analysis.

Fig. 6 displays the mass errors for the isotone chains $N=78$ to 89 , and their Fourier analysis.

Many isotopic chain exhibit similar oscillatory patterns in the mass errors. However, a Fourier decomposition is always crude because there are only a few points, typically between 15 and 30, in each chain.

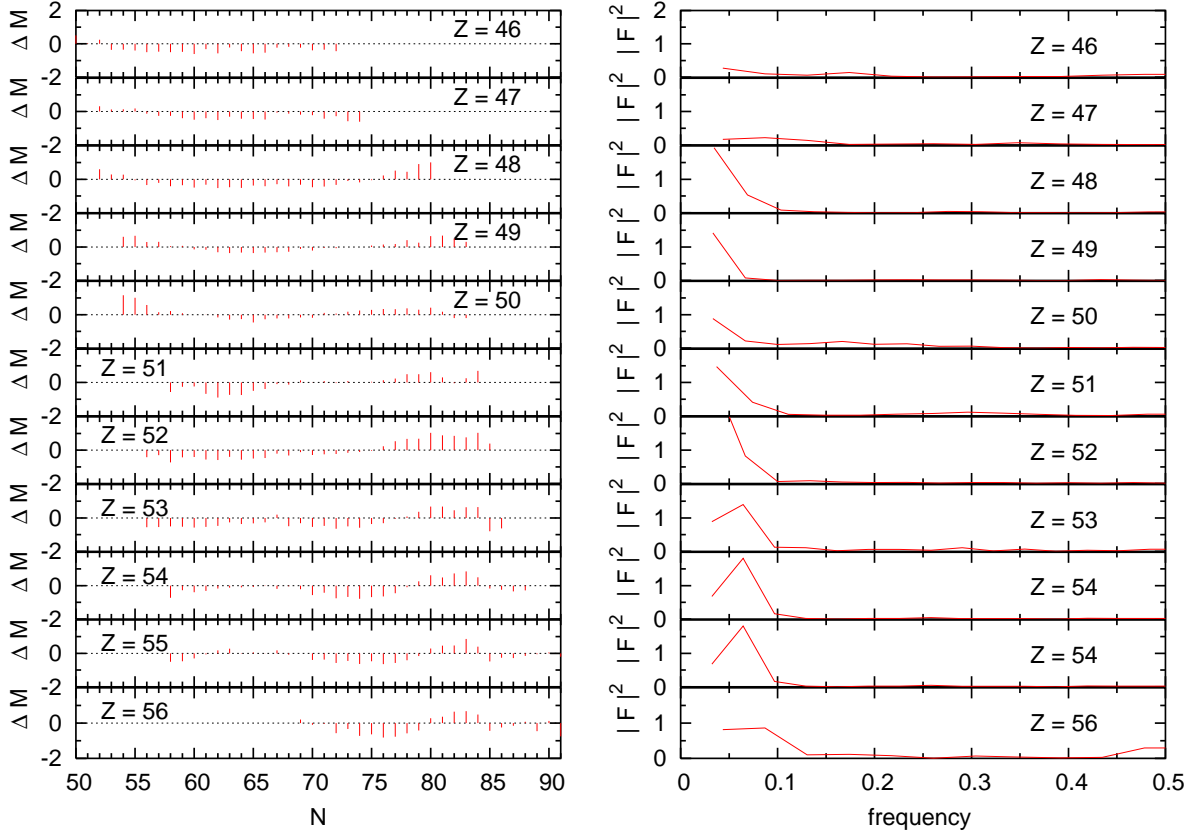


FIG. 3: Mass errors in the isotope chains $Z=46$ to 56 , and their Fourier analysis.

B. Fixed A and T_z

To map the mass error data in term of variables with the maximum possible number of nuclei along each chain, the following transformation is employed

$$\tilde{A} = \sqrt{2}(N \sin\theta + Z \cos\theta), \quad \tilde{T}_z = \sqrt{2}(N \cos\theta - Z \sin\theta). \quad (1)$$

Both \tilde{A} and \tilde{T}_z are, by construction, integer numbers. To avoid introducing artificial noise, the data are *softened* by the interpolation of mass errors for *unphysical* values of \tilde{T}_z , \tilde{A} , i.e. those with \tilde{T}_z even and \tilde{A} odd, or viceversa. This process is necessary to eliminate the large number of zeros which are induced by the transformation, which create artificial high frequency noise in the data.

The present definition has the advantage that, for $\theta = 45^\circ$, $\tilde{A} = A$, $\tilde{T}_z = 2T_z$. There are seven values of T_z which have more than 40 nuclei with measured masses. They are $2T_z = 5, 6, 7, 8, 16, 17, 18$. Their mass differences ΔM are plotted as a function of the mass

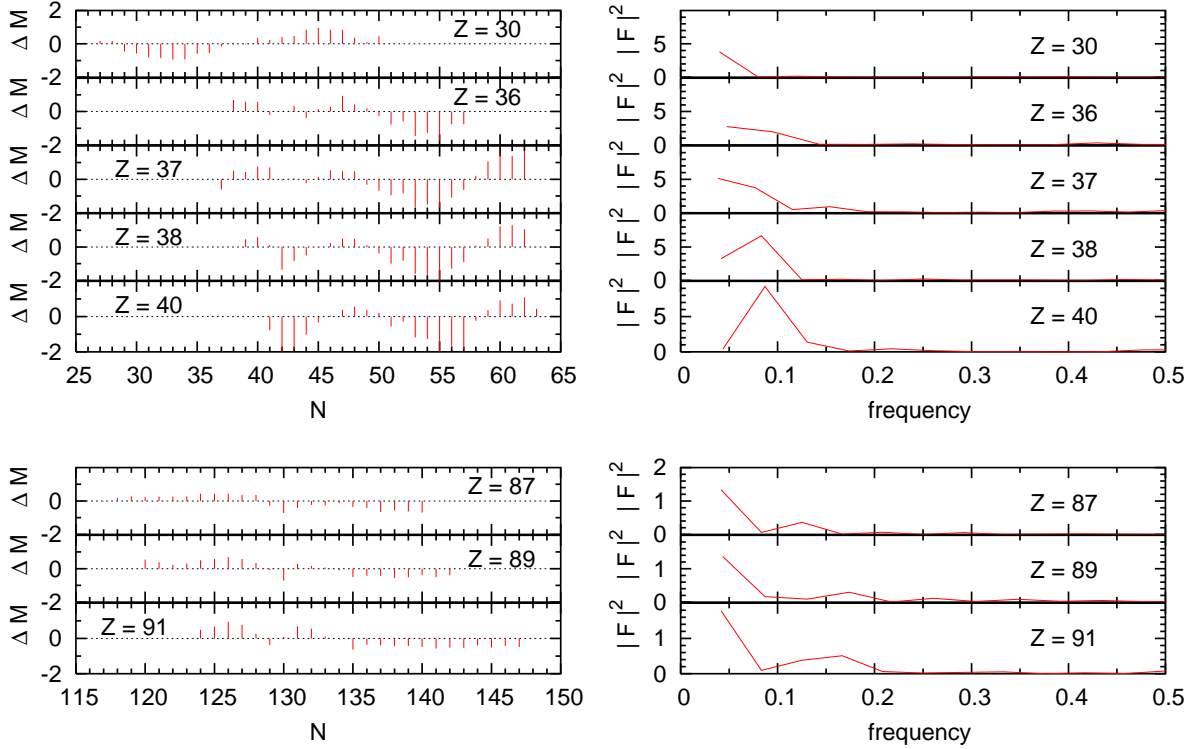


FIG. 4: Mass errors in the isotope chains with $Z = 30, 36, 37, 38, 40, 87, 89, 91$, and their Fourier analysis.

number A in the seven inserts shown in Fig. 7. The clustering of negative and positive errors is evident, exhibiting the presence of residual correlations between the mass errors and the atomic and neutron numbers (Z, N), or, equivalently, with the isospin projection and the mass numbers.

The squared amplitudes of the Fourier transforms of the mass differences are shown in Fig. 8. For the first four isotopic chains ($2T_z = 5, 6, 7, 8$) there is a prominent peak at $f \approx 0.033$, i.e. a period $\Delta A \approx 30$, which is about one third the size of each set of nuclei. The remaining three chains exhibit also a peak at low frequencies, but lower and wider.

In order to underline the relevance of just three frequencies in the mass error distribution, in Fig. 9 the mass errors are plotted as function of A , for $2T_z = 6$ (left), and 8 (right), in the top panel. The middle panel exhibits the distribution obtained including only three low frequencies: $f = 0.011, 0.022, 0.033$. The second is the most important, with a period $\Delta A \approx 46$.

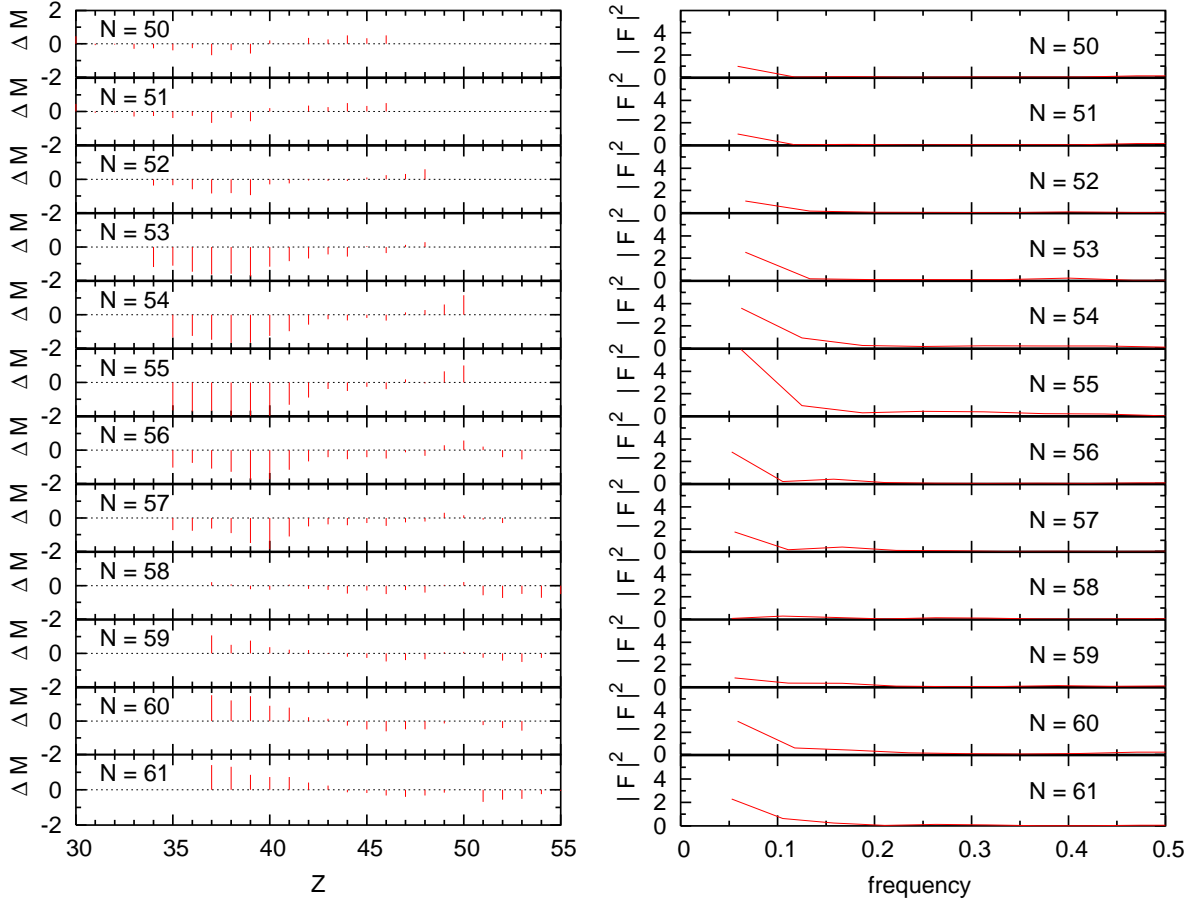


FIG. 5: Mass errors in the isotone chains $N=50$ to 61 , and their Fourier analysis.

C. Rotated \tilde{A} and \tilde{T}_z

We found that the best orientation, in order to have as many isotopes as possible with the same \tilde{T}_z , is $\theta = 56^\circ$. With this transformation, there are 174 isotopes with $\tilde{T}_z = 0$.

Figure 10 displays the mass errors for 7 values of \tilde{T}_z , from $\tilde{T}_z = -4$ to 2 . The regularities seen in Fig. 2 as regions with the same gray tone are seen here in the different plots, as a bunch of nuclei with similar positive or negative mass differences, for the same \tilde{A} region. Besides the two large groups with positive and negative mass errors below $\tilde{A} = 50$, there are evident regions with negative errors close to $\tilde{A} = 100$, and with positive mass differences for $150 < \tilde{A} < 200$.

A Fourier analysis of the previous results is presented in Fig. 11. It is clear that for all the chains a few low frequencies dominate the spectrum. In some chains there are also

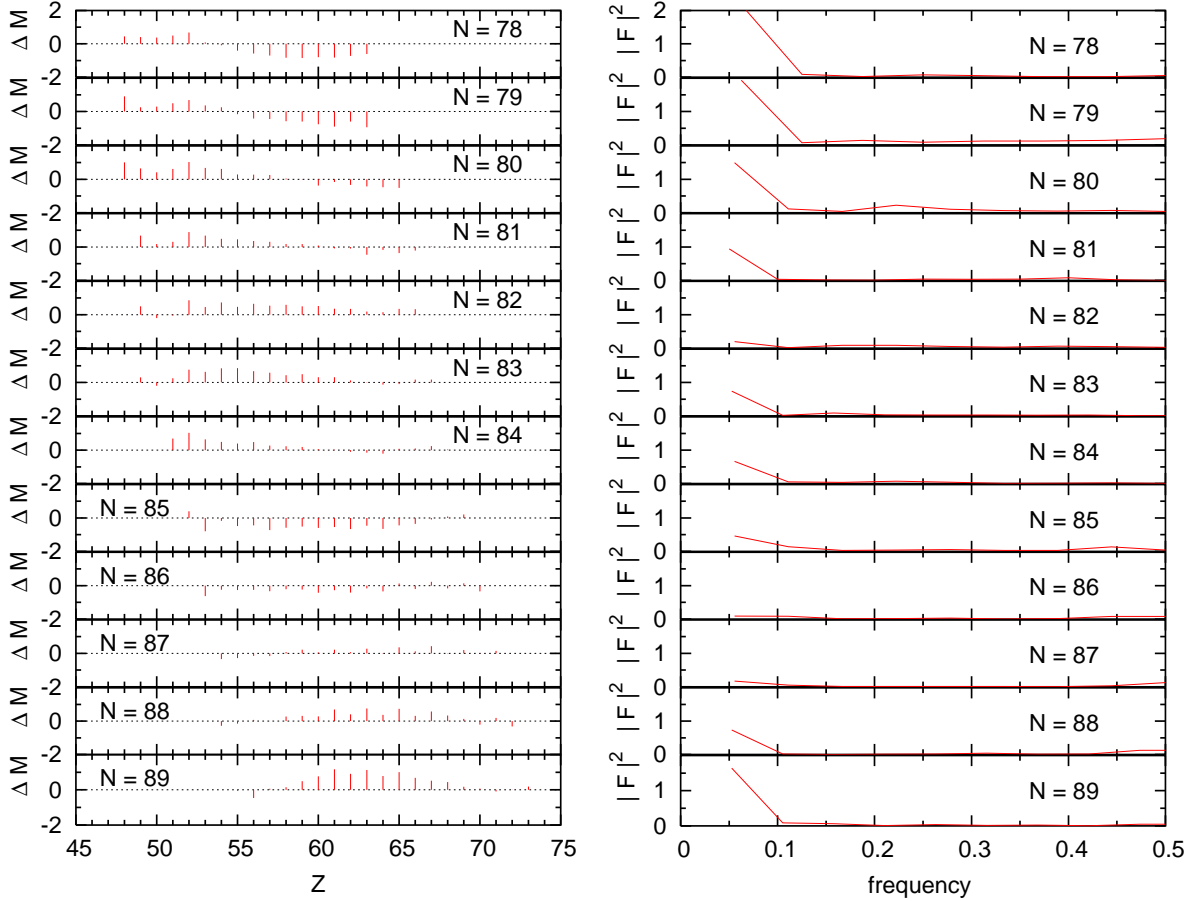


FIG. 6: Mass errors in the isotone chains $N=78$ to 89 , and their Fourier analysis.

some high frequencies which are relevant, while for $\tilde{T}_z = 0$ their contribution is small. These high frequencies, close to $f = 0.5$, refer to oscillations with period 2, i.e. strong fluctuations between one nucleus and its closest neighbors.

In Fig. 12 the contribution of very few frequencies to the mass differences, for the chains with $\tilde{T}_z = -2, -1, 0$ and 1 are presented. The upper panels show the full sequences of mass differences, the medium panels the contribution of the four frequencies with the largest amplitudes, and the lower panels the remaining mass errors. In all the cases it is apparent that the regularities are very significant, and that their subtraction would lead to important improvements in mass calculations.

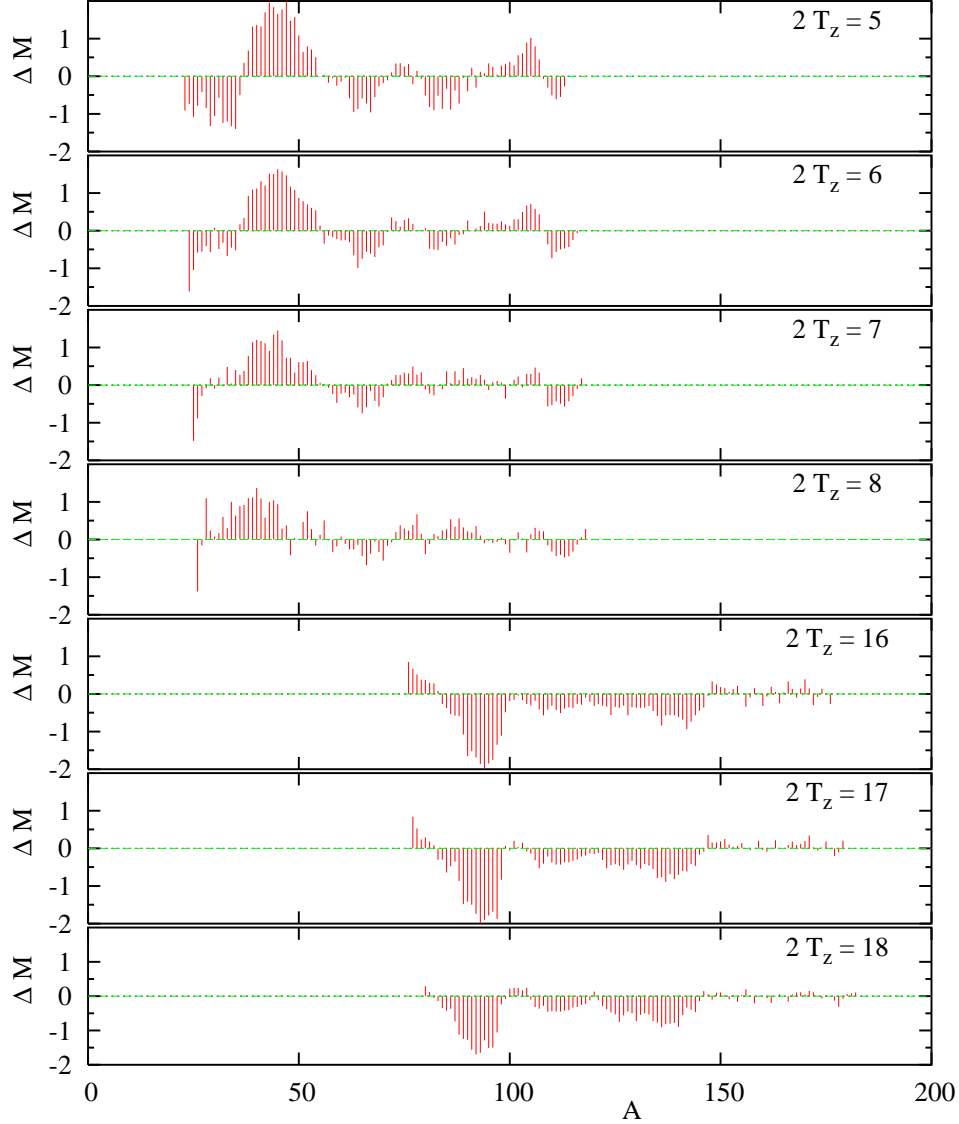


FIG. 7: Mass differences as functions of A , for seven T_z values.

D. All data aligned

Plotting the mass differences for different Z , Fig. 13 top, and for different N , Fig. 13 bottom, is very common in mass calculations. Both plots exhibit some degree of structure. In this way we obtain a plot of mass differences as a function of Z , with all the isotopes plotted along the same vertical line, see Fig. 13. The difficulty in quantifying these regularities lies in the simple fact that there are many nuclei with a given N or Z . For this reason in the previous subsections we have analyzed the data using different cuts. Another way to organize

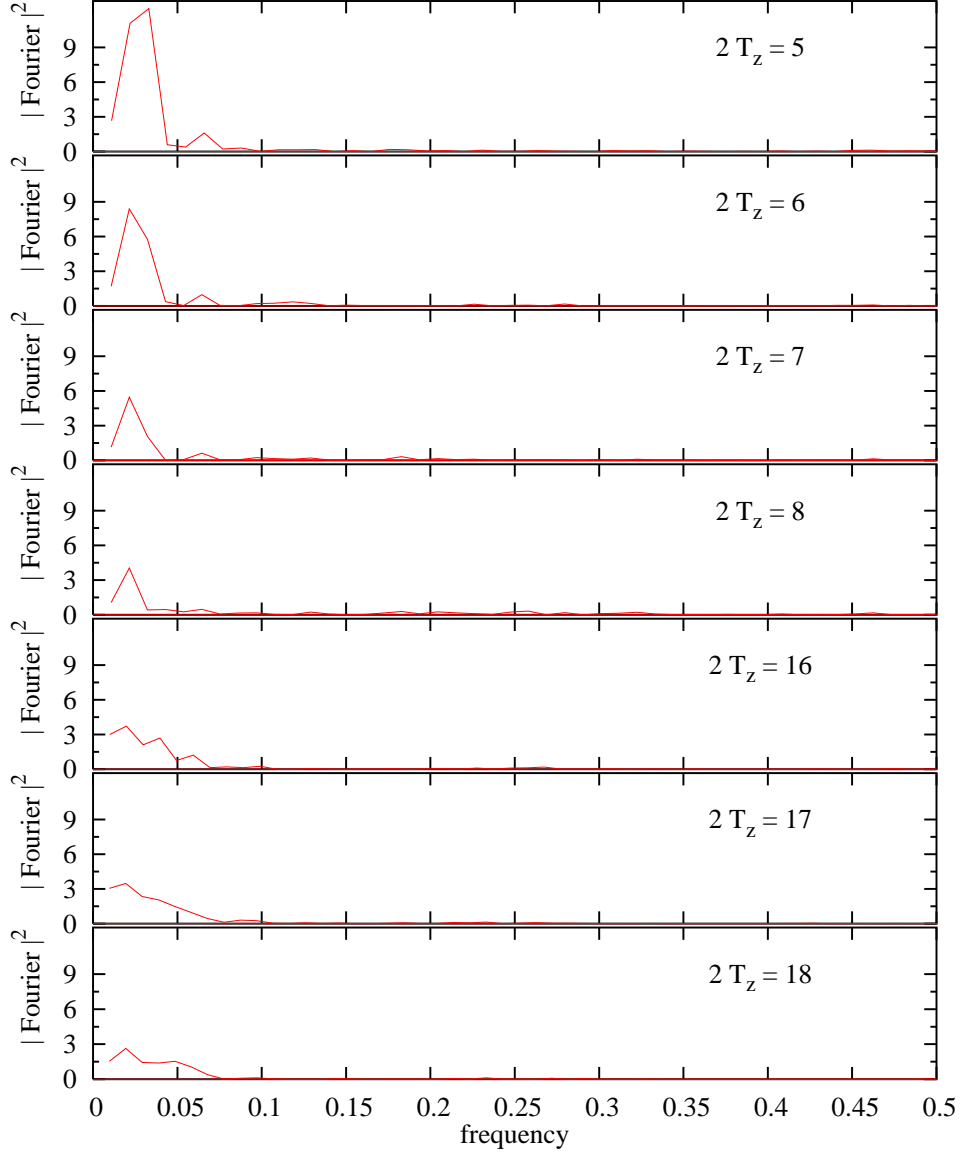


FIG. 8: Squared amplitudes of the Fourier transforms of the mass differences, plotted as functions of A , for seven T_z values.

the 1654 nuclei with measured masses reported in Möller et al. is to order them in a single list, numbered in increasing order. To avoid jumps, we have ordered the isotopes in even Z following the increase in N , and those isotopes with odd Z starting from the largest N , and going on in decreasing order. The middle panel exhibits the same mass differences plotted against the order number, from 1 to 1654. It provides a univalued function, whose Fourier transform can be calculated. The squared amplitudes are presented in Fig. 14. Unlike

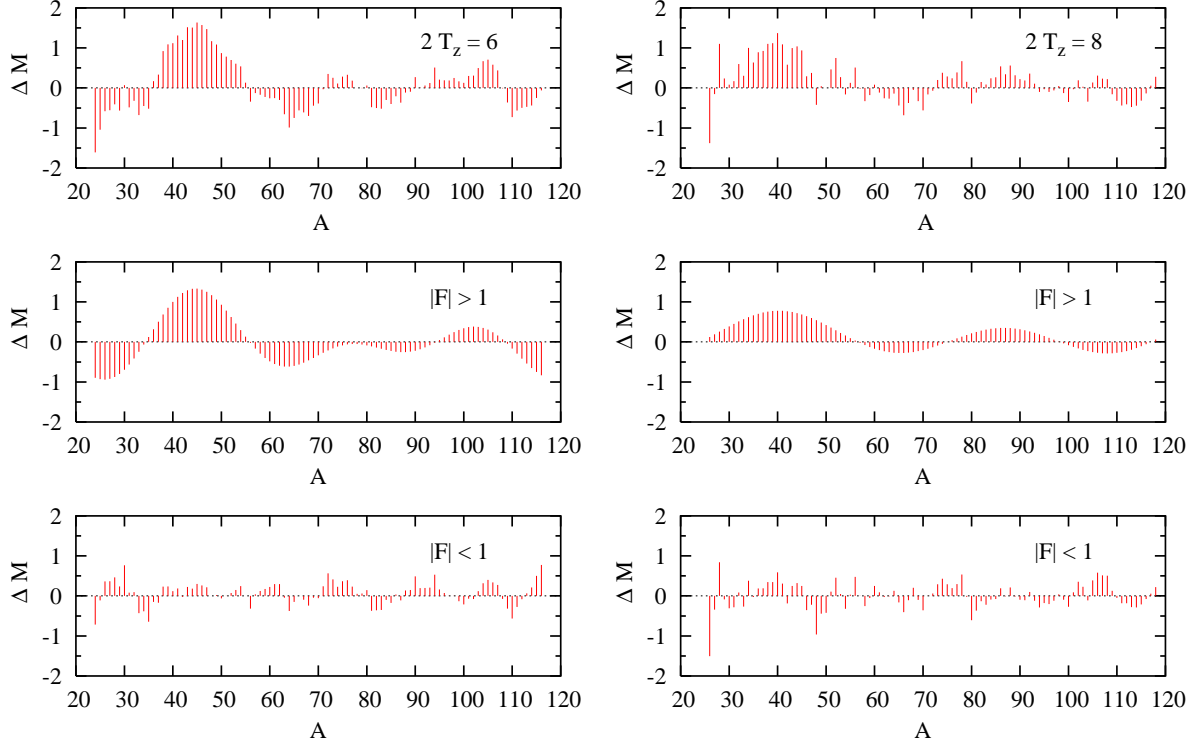


FIG. 9: Mass differences as functions of A , for $2T_z = 6$ (left), and 8 (right). The middle panels show the distribution for only the few frequencies with Fourier amplitudes larger than 1, the lower panels the distribution for all the remaining frequencies.

the cuts for given N , Z , A or T_z , the fully ordered data have many different frequencies with large Fourier amplitudes. The most remarkable characteristic is the flat distribution of amplitudes for $-4 < \log(f) < -2.5$, which could be interpreted as white noise.

Removing those frequencies with the largest Fourier components helps very little in this case. Figure 15 shows the mass differences plotted as function of the order index, and the results of leaving only the frequencies with amplitudes $|F|$ larger (or smaller), than 1, 2 and 3. While keeping only $|F| \leq 1$ looks like white noise, there are too many frequencies with $|F| > 1$, and no simple conclusion can be extracted from this truncation. On the opposite side, there are very few frequencies with amplitudes larger than 3, but what remains is nearly as complex as the original set of data.

From the analysis presented in this section, we can conclude that there are conspicuous correlations in the mass differences obtained by Möller et al, whose periodic character is clearly exhibited by the Fourier analysis of different cuts. Ordering all the data in a single

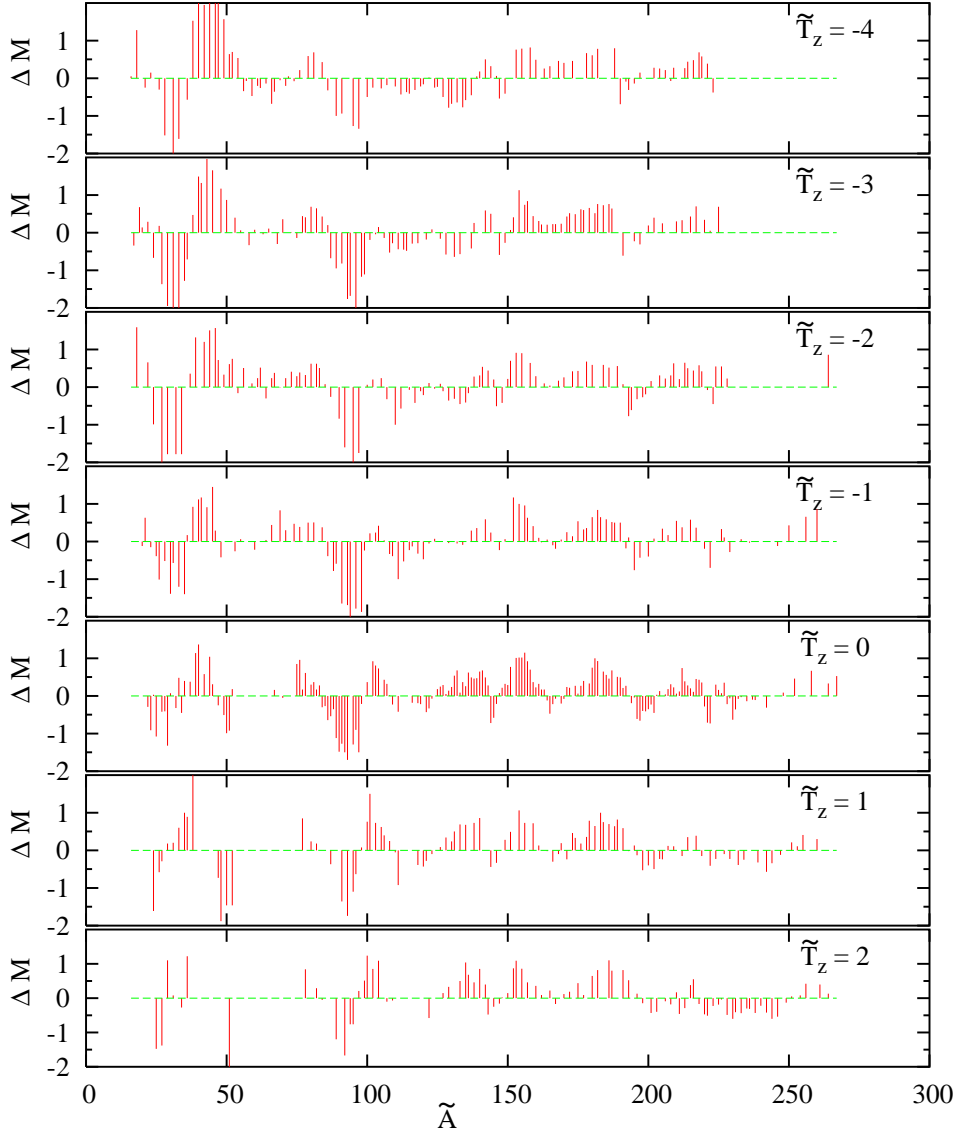


FIG. 10: Mass differences as functions of \tilde{A} , for seven \tilde{T}_z values.

succession does not seem useful for this type of study. It could be worth studying the slope of the squared amplitudes against the frequencies in a log-log plot, which in another context was found to offer a signature of quantum chaos [10]. It is left for a future contribution [11]

III. REMOVING THE REGULARITIES

Having established that there are patent regularities in the differences between the masses calculate by Möller at al and the measured ones, we will proceed to elliminate them in a

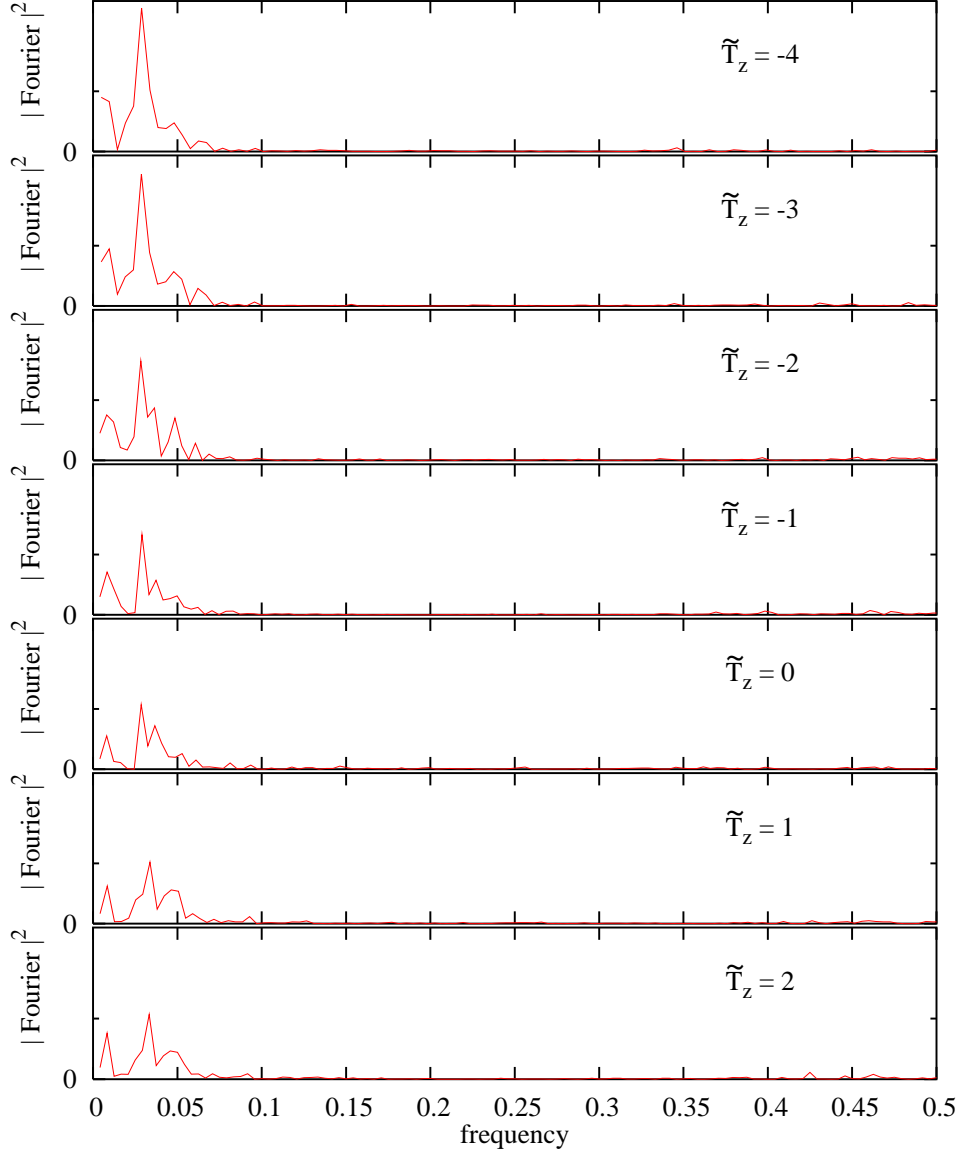


FIG. 11: Squared amplitudes of the Fourier transforms of the mass differences, plotted as functions of the frequency, for seven \tilde{T}_z values.

simple way, by removing the two frequencies which contribute the most to the mass errors as functions of N and Z . We introduce an amplitude and a phase for each frequency, having a total of six parameters for protons and six for neutrons. The functions which minimize the errors are:

$$\Delta_1(N) = .30 \sin(2\pi.012N + .284) + .20 \sin(2\pi.047N + 1.06) \quad (2)$$

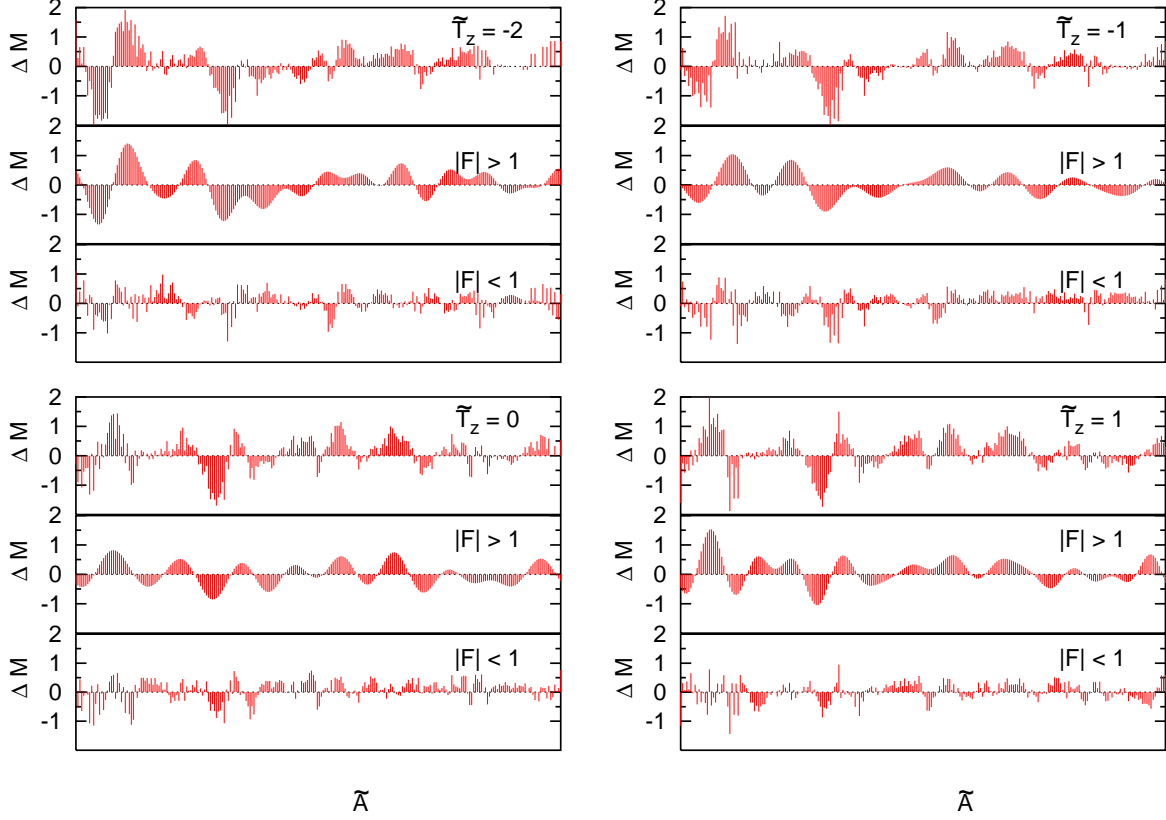


FIG. 12: Mass differences as functions of \tilde{A} , for $\tilde{T}_z = -2$ (upper left), -1 (upper right), 0 (lower left) and 1 (lower right). The middle panels show the distribution for only the few frequencies with Fourier amplitudes larger than 1, the lower panels the distribution for all the remaining frequencies.

$$\Delta_1(Z) = .23 \sin(2\pi.020Z - 0.83) + .10 \sin(2\pi.053Z + 3.74) \quad (3)$$

fit including all nuclei

$$\Delta_2(N) = .21 \sin(2\pi.011N + 0.86) + .34 \sin(2\pi.049N + 0.17)$$

$$\Delta_2(Z) = .14 \sin(2\pi.025Z - 0.74) - .19 \sin(2\pi.075Z - 5.53)$$

$$\Delta_2(N, Z) = \Delta_2(N) + \Delta_2(Z) \quad (4)$$

fit including only nuclei with $A \geq 65$

$$\Delta_3(N) = .65 \sin(2\pi.009N + 2.03) + .19 \sin(2\pi.047N + 1.00)$$

$$\Delta_3(Z) = 2.90 \sin(2\pi.018Z - 3.51) + 2.61 \sin(2\pi.019Z - 0.74)$$

$$\Delta_3(N, Z) = \Delta_3(N) + \Delta_3(Z) \quad (5)$$

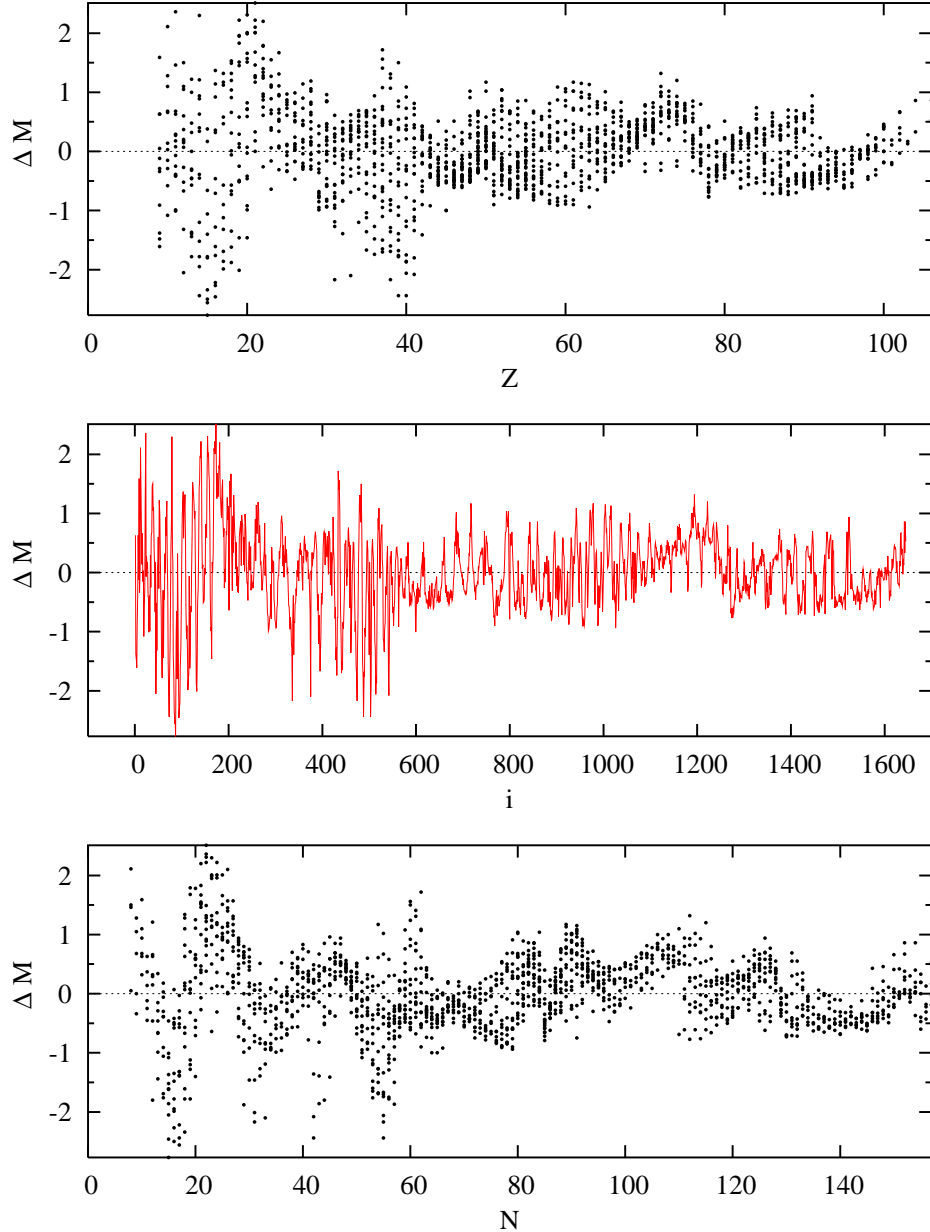


FIG. 13: Mass differences plotted as function of Z (top), N (bottom), and of an ordered list (middle)

Δ_1 are functions only of N or Z , and were adjusted using six parameters, optimized for the 1350 nuclei with $A \geq 65$. Δ_2 and Δ_3 are obtained by including at the same time the corrections in Z and N , for all the nuclei in the first case, and for those with $A \geq 65$ in the second. The fitted frequencies are typically between 0.01 and 0.05, in agreement with the dominant Fourier frequencies found in the previous section.

The effect of removing these sinusoidal components as functions of N and Z is shown in

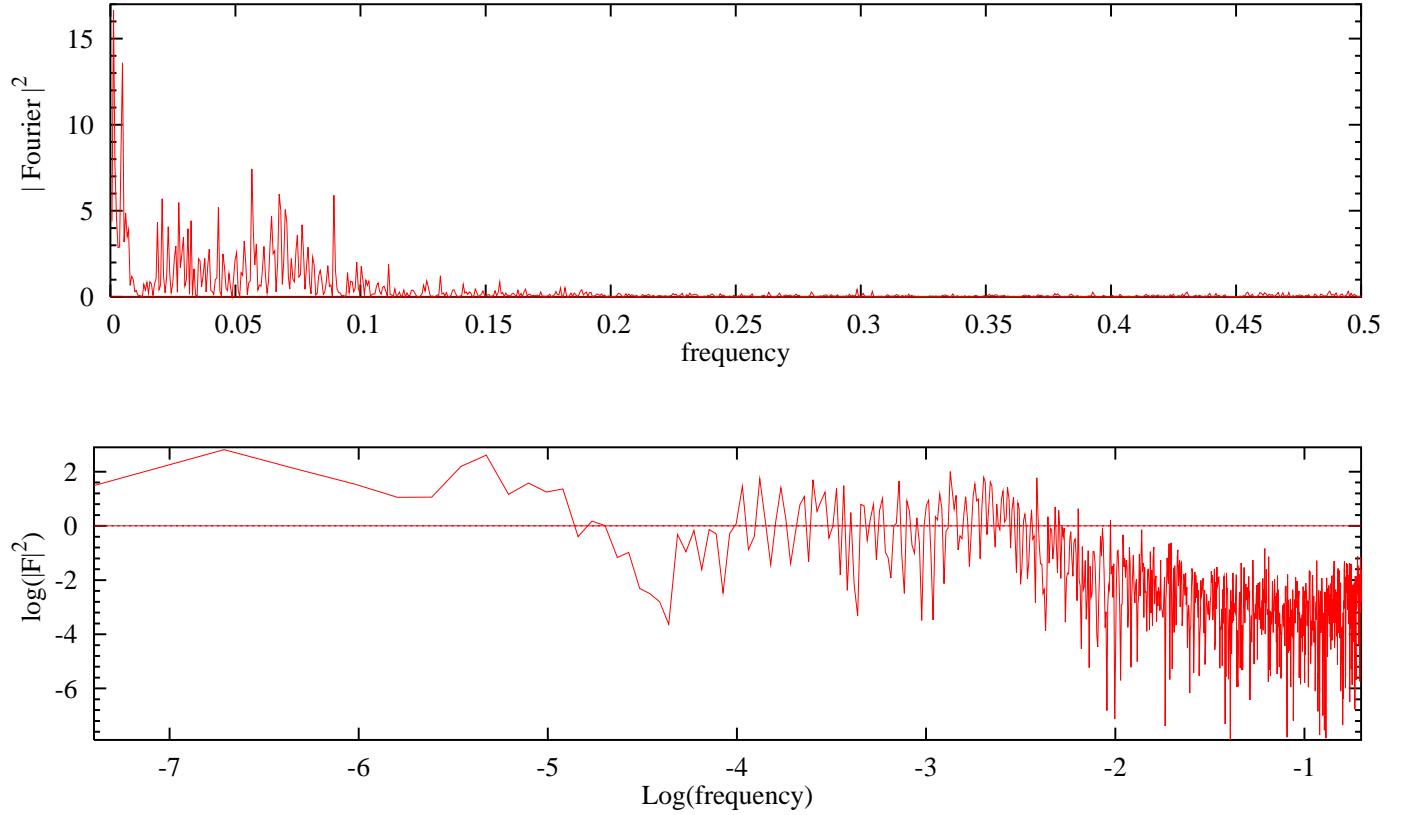


FIG. 14: Squared amplitudes of the Fourier transforms of the mass differences, plotted as functions of the order parameter (top). Logarithm of squared amplitudes of the Fourier transforms of the mass differences N (bottom)

Fig. 16, for those nuclei with masses larger than 65. While the regular pattern is more apparent as a function of N , on the right hand side panels, in both cases the ‘corrected’ masses are more compact and compressed at smaller errors.

Obtaining a better fit of the known nuclear masses by the inclusion of six or twelve extra variables is by no means surprising. However, the use of sinusoidal functions of N and Z is strongly motivated by the data themselves. The fit does not only reduce the overall error, but makes the double peak in the error distribution disappear, as shown in Fig. 17 for all the nuclei, and in Fig. 18 for nuclei with $A \geq 65$. In both figures the error width reduction is

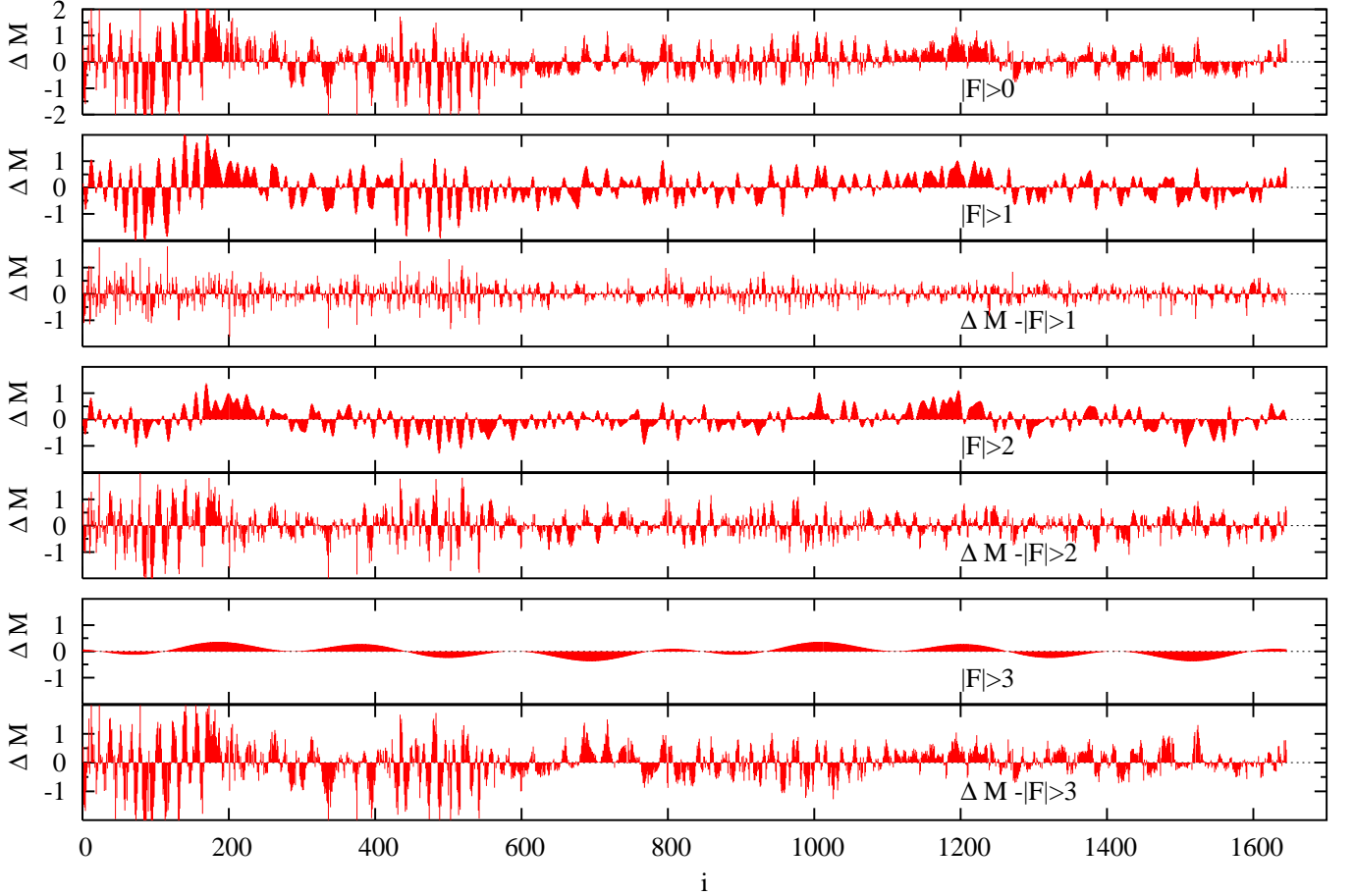


FIG. 15: Mass differences plotted as an ordered list (top). The pair of plots show the mass error function recovered when only those Fourier amplitudes larger than 1 are considered, and the mass error function which remains when the larger Fourier amplitudes are removed. The other plots show the same for amplitudes larger than 2, 3.

evident, as well as the concentration of the mass differences around zero, with a single peak. The continuous curve represents a Gaussian curve with the same width and normalization. After removing the oscillatory components, the r.m.s. mass errors is reduced from 0.681 MeV to 0.597 MeV for all nuclei, and from 0.534 MeV to 0.462 MeV for nuclei with $A \geq 65$.

IV. FINAL REMARKS

In the present study we have shown that the differences between the masses calculated by Möller et al and the measured ones have a well defined oscillatory component as function of N and Z , which can be removed with an appropriate fit, significantly reducing the error width, and concentrating the error distribution on a single peak around zero.

The remaining correlations could originate in the microscopic terms in the mass formula, which are evaluated using the Strutinsky method [12]. The possible removal of these effects by a refinement of the Strutinsky method is currently under analysis [11].

It is worth investigating if, after removing the oscillatory components, the remaining mass differences display the intrinsic chaotic signatures suggested in [5]. We have not found a clear answer yet, although the tendency to generate a Gaussian distribution of the mass errors could point in this direction. It must be pointed out, however, that the new fits do not exhibit any preference for a $A^{-1/3}$ dependence, which in [5] was pointed out as a sign of chaos. It remains to be seen whether a more reliable mass formula can be derived using these ideas [11], and whether nuclear masses indeed display a remnant of chaotic dynamics.

Acknowledgements

Acknowledgements: Relevant comments by R. Bijker, O. Bohigas, J. Dukelsky, J. Flores, J.M. Gomez, P. Leboeuf, S. Pittel, A. Raga, P. van Isacker, and A. Zuker are gratefully acknowledged. This work was supported in part by Conacyt, México.

-
- [1] S. Åberg, *Nature* **417**, 499 (2002).
 - [2] P. Möller, J.R. Nix, W.D. Myers, W.J. Swiatecki, *At. Data Nucl. Data Tables* **59**, 185 (1995).
 - [3] J. Duflo, *Nucl. Phys. A* **576**, 29 (1994); J. Duflo and A. P. Zuker, *Phys. Rev. C* **52**, R23 (1995).
 - [4] S. Goriely, F. Tondeur, and J.M. Pearson, *Atom. Data Nucl. Data Tables* **77**, 311 (2001).
 - [5] O. Bohigas, P. Leboeuf, *Phys. Rev. Lett.* **88**, 92502 (2002).
 - [6] E.P. Wigner, *Statistical Theories of Spectra: Fluctuations*, Academic, New York (1965).

- [7] Víctor Velázquez, Jorge G. Hirsch, and Alejandro Frank, *Rev. Mex. Fís.* **49** S. 1 (2003) in press.
- [8] M.L. Mehta, *Random Matrices*, Academic Press, London (1990)
- [9] Víctor Velázquez, Alejandro Frank, and Jorge G. Hirsch, Proc. of the workshop *Computational and Group Theoretical Methods in Nuclear Physics*, Playa del Carmen, Mexico, February 18 - 22, 2003, World Scientific, Singapore, in press.
- [10] A. Relaño, J.M.G. Gómez, R.A. Molina, J. Retamosa and E. Faleiro, *Phys. Rev. Lett.* **89** (2002) 244102.
- [11] Víctor Velázquez, Alejandro Frank, and Jorge G. Hirsch, in preparation.
- [12] M. Brack, Jens Damgaard, A.S. Jensen, H.C. Pauli, V.M. Strutinsky, C.Y. Wong, *Rev. Mod. Phys.* **44** (1972) 320; V.M. Strutinsky and F.A. Ivanjuk, *Nucl. Phys.* **A 255** (1975) 405.

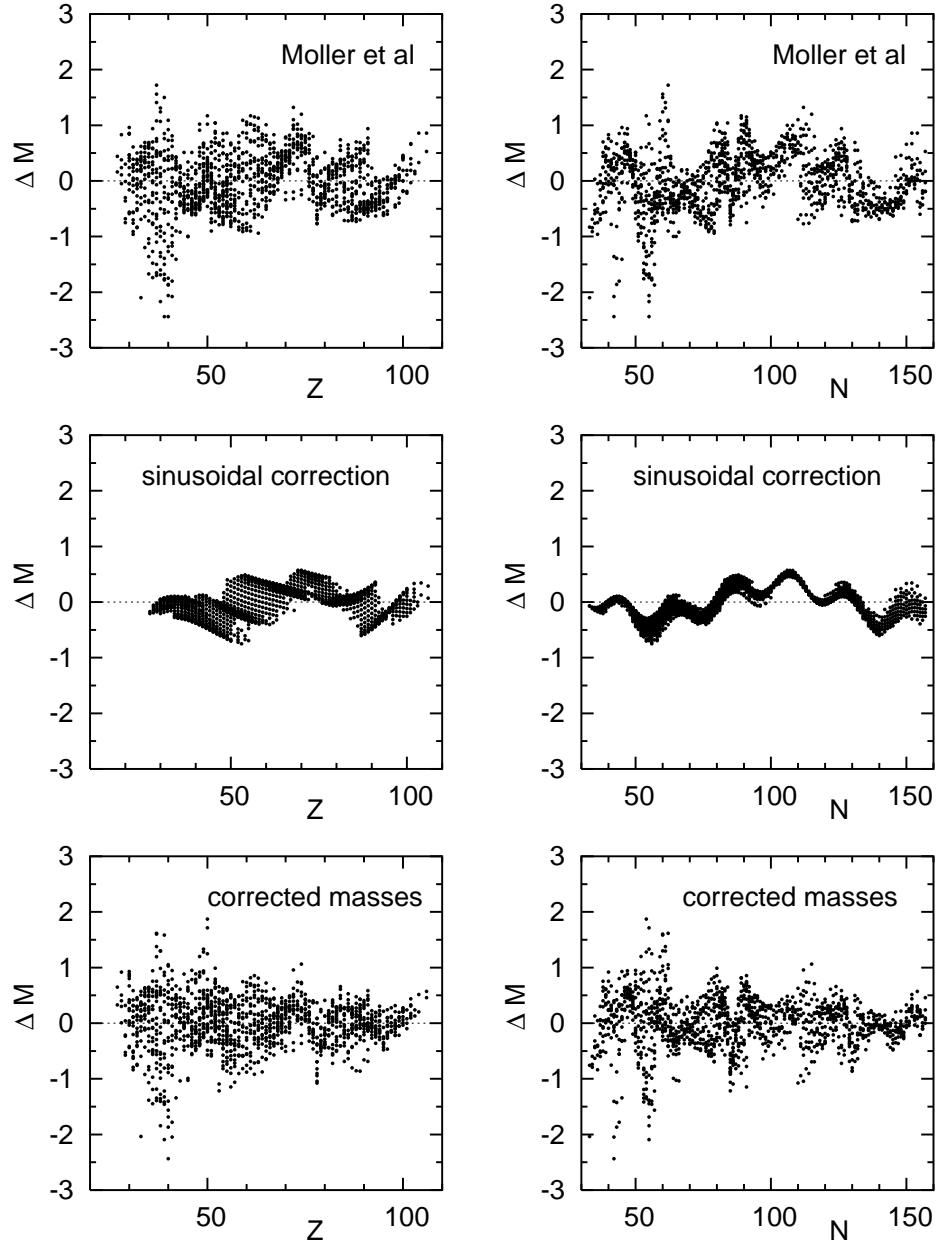


FIG. 16: Mass differences plotted as function of Z (left) and N (right), for $A \geq 65$. The upper panels exhibit the Möller et al. results, the intermediate ones the sinusoidal corrections, and the lower panels the corrected mass differences.

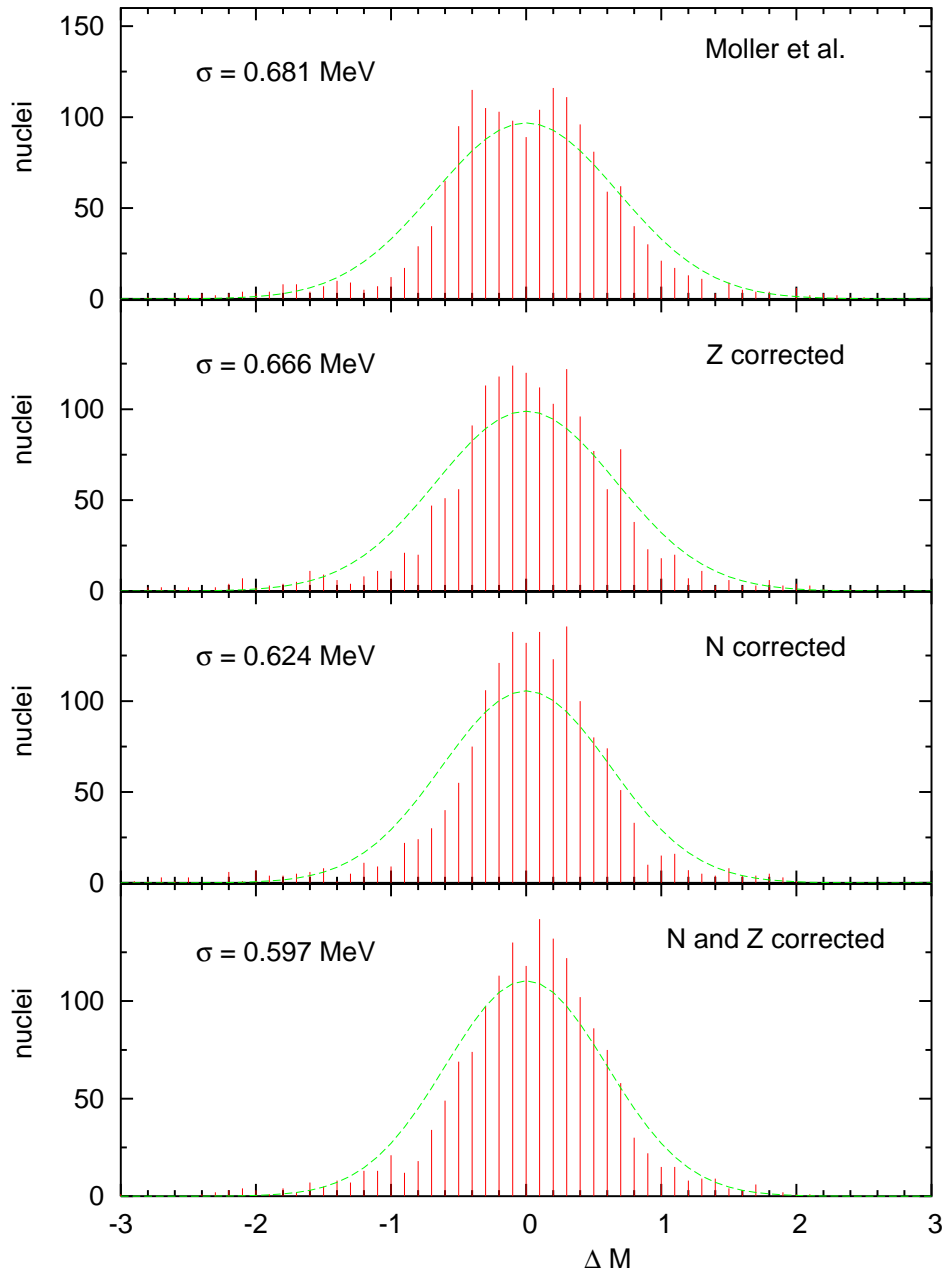


FIG. 17: Distribution of mass differences, from Möller et al., corrected with a sinusoidal function of Z, of N, and of Z and N.

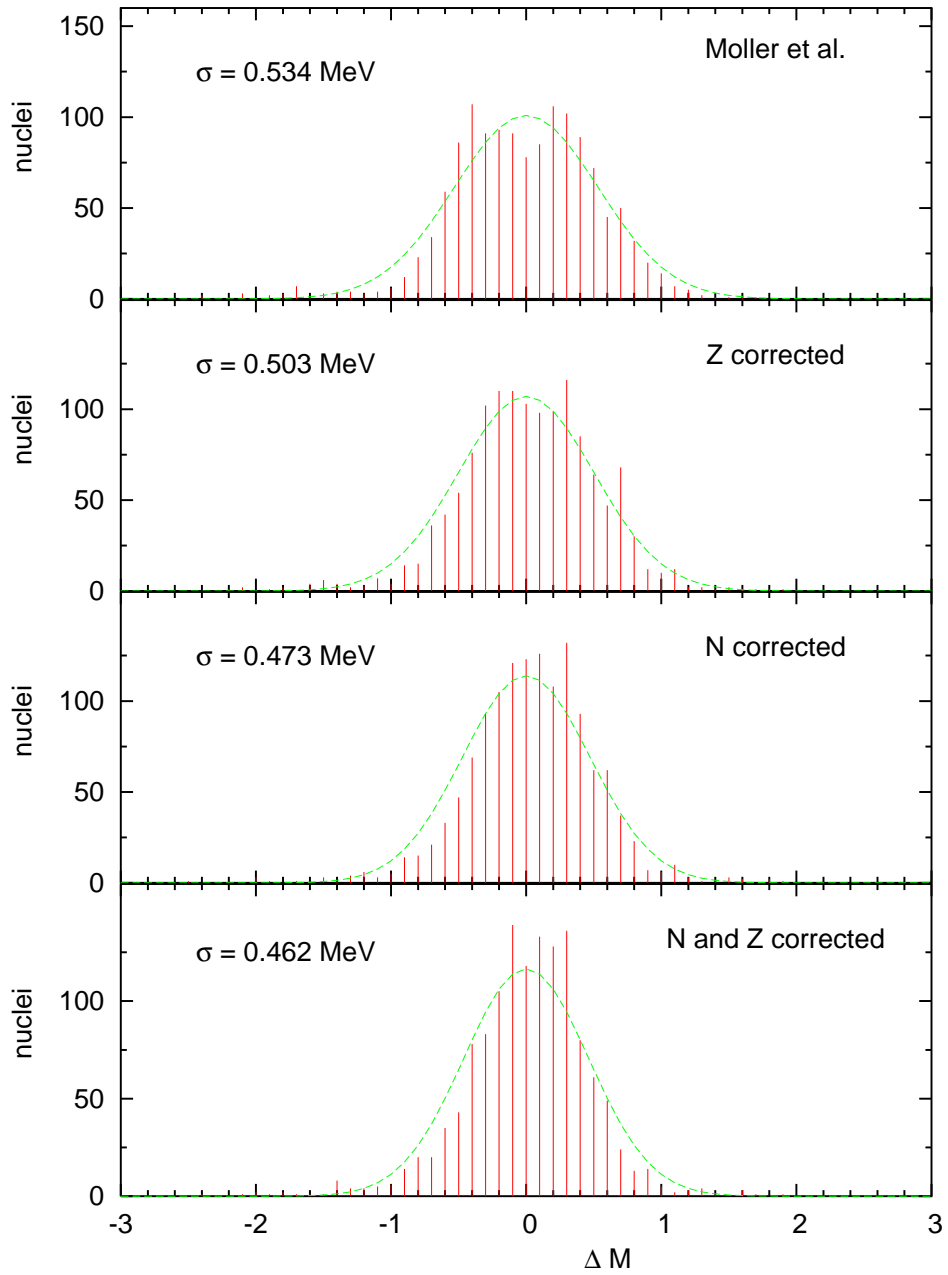


FIG. 18: Distribution of mass differences for $A \geq 65$, from Möller et al., corrected with a sinusoidal function of Z, of N, and of Z and N.